Influence of rectilinear vs radial advection on the yield of A + B → C reaction fronts: A comparison

Fabian Brau (iD), and A. De Wit (iD)

View Online **Export Citation** **CrossMark**

Influence of rectilinear vs radial advection on the yield of A + B → C reaction fronts: A comparison

View Online   Export Citation   CrossMark

Fabian Brau[a] [iD] and A. De Wit[b] [iD]

AFFILIATIONS

Université libre de Bruxelles (ULB), Nonlinear Physical Chemistry Unit, Faculté des Sciences, CP231, 1050 Brussels, Belgium

[a]E-mail: fabian.brau@ulb.ac.be
[b]Author to whom correspondence should be addressed: adewit@ulb.ac.be

ABSTRACT

In the presence of advection at a constant flow rate in a rectilinear geometry, the properties of planar A + B → C reaction fronts feature the same temporal scalings as in the pure reaction–diffusion case. In a radial injection geometry where A is injected into B radially at a constant flow rate Q, temporal scalings are conserved, but the related coefficients depend on the injection flow rate Q and on the ratio γ of initial concentrations of the reactants. We show here that this dependence of the front properties on the radial velocity allows us to tune the amount of product obtained in the course of time by varying the flow rate. We compare theoretically the efficiency of the rectilinear and radial geometries by computing the amount of product C generated in the course of time or per volume of reactant injected. We show that a curve $\gamma_c(Q)$ can be defined in the parameter space (γ, Q) below which, for similar experimental conditions, the total amount of C is larger in the radial case. In addition, another curve $\gamma^*(Q) < \gamma_c(Q)$ can be defined such that for $\gamma < \gamma^*$, the total amount of C produced is larger in the radial geometry, even if the production of C per unit area of the contact interface between the two reactants is larger in the rectilinear case. This comes from the fact that the length of the contact zone increases with the radius in the radial case, which allows us to produce *in fine* more product C for a same injected volume of reactant or in reactors of a same volume than in the rectilinear case. These results pave the way to the geometrical optimization of the properties of chemical fronts.

Published under license by AIP Publishing. https://doi.org/10.1063/1.5135292

I. INTRODUCTION

Traveling chemical fronts are ubiquitously encountered in numerous applications ranging from ecology, disease spreading, environment, stock market dynamics, and also genuinely in chemical and biological systems.[1,2] In the vast class of chemical fronts, A + B → C fronts have been extensively studied and characterized theoretically because, depending on the interpretation of A and B, they underline many applications.[3–6] Such fronts typically develop when a zone rich in A is put in contact along a given interface with a zone rich in B. In the absence of any flow, the interplay between the A + B → C kinetics and the diffusive transport of the reactants toward the reaction zone induces a front, the properties of which have been largely studied. In particular, Gálfi and Rácz have shown that, for the rectilinear case in which the initial contact interface between A and B is a line, the temporal evolution of the position of the front x_f scales as $t^{1/2}$, while the production rate R and the

width of the front w vary as $t^{-2/3}$ and $t^{1/6}$, respectively.[7] Meanwhile, these scalings have been well demonstrated experimentally.[8,9] If such fronts are advected at a constant speed, the above scalings remain unchanged in the reference frame moving at the imposed speed.

Even though some experiments have noted that curvature can have an influence on the properties of such A + B → C fronts,[10–12] the radial reaction–diffusion (RD) case where A diffuses out in a radial way into a pool of B such that the contact interface is an expanding circle has received less attention. This is related to the impossibility to sustain indefinitively a constant concentration of A at the initial point source because of diffusion and thus to find the asymptotic properties of such radial fronts. Some stamp experiments have studied interesting transient reaction–diffusion patterns when gel stamps of A of various shapes are put in contact with a gel containing B.[13] Similarly, theoretical work has computed the transient reaction–diffusion properties of a localized source of A that is finite (or acts
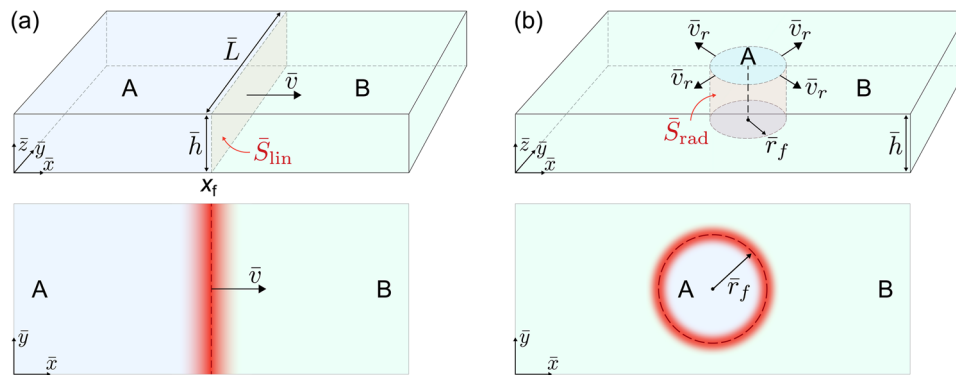
FIG. 1. Three-dimensional schematics and top view of A + B → C reaction–diffusion–advection fronts. The red zone features the product C generated by the A + B → C reaction. (a) Rectilinear geometry where the front moves at a constant speed, $\bar{\boldsymbol{v}} = \bar{v}\,\boldsymbol{e}_x$, and where the constant contact area between the two reactants A and B reads $\bar{S}_{\text{lin}} = \bar{h}\bar{L}$. (b) Radial geometry where the front moves with a speed that decreases with the radial distance, $\bar{\boldsymbol{v}} = \bar{v}_r(\bar{r})\,\boldsymbol{e}_r$ with $\bar{v}_r \sim 1/\bar{r}$, and where the contact area between the two reactants A and B increases with the radial distance: $\bar{S}_{\text{rad}} = 2\pi\bar{h}\bar{r}_f$.

for a given finite time) consumed in a sea of B.[4,14,15] Nevertheless, no asymptotic scalings have been computed as the mathematical long time limit problem of a point source of species A diffusing radially in a sea of B is ill-posed.

Interest for radial A + B → C fronts has sparked again recently, thanks to experimental studies on precipitation patterns obtained in confined geometries when a solution of a reactant A is injected radially at a constant flow rate into a solution of reactant B and a precipitation A + B → C(s) reaction takes place. Various complex precipitation patterns have been observed,[16–19] paving the way to renewed interest for the effect of flows on reaction fronts. The fact that A is injected continuously at the center of the quasi-2D reactor initially filled with B allows to maintain a source of A with constant concentration at the central point source boundary. Physically, this allows to feed the A + B → C front with refreshed A while it expands radially. Mathematically, injection solves the ill-posed boundary condition at the source point of the pure RD problem and allows to compute the long time asymptotic scalings of radially advected A + B → C fronts. In particular, it has been shown that, for long times, the temporal scalings of the properties of two-dimensional radial reaction–diffusion–advection (RDA) A + B → C fronts are the same as those of the rectilinear RD case, i.e., the radial position of the front r_f scales as $t^{1/2}$, while the production rate R and the width of the front w still vary as $t^{-2/3}$ and $t^{1/6}$, respectively.[3,5] Advection, however, impacts the proportionality factors that are a function of the flow rate Q, which suggests that tuning Q can provide flow control of the front properties. Recently, these results have been extended to three-dimensional (3D) systems. The novelty for a 3D radial spreading is that the dynamics eventually reaches a stationary state where the front position is fixed and the concentration profiles of A and B do not depend on time. Before reaching this stationary state, the system evolves through an early-time regime and a transient regime, both characterized by well-defined and different scalings.[6]

In this context, we explore here the geometrical control of A + B → C fronts in flow conditions by analyzing the difference in the yield of the reaction in a 3D rectilinear displacement vs a radial injection along an expanding cylinder (see Fig. 1). To do so, we

compute analytically the amount of product C generated when a reactant A is injected into the other reactant B at a constant flow rate in rectilinear and radial geometries, respectively. In rectilinear systems, the quantity of product increases as $t^{1/2}$ and is directly proportional to the area of the contact zone between the two reactants A and B. In the radial geometry, the area of the contact zone increases with the radius of the expanding reaction circle at a speed that depends on the injection flow rate and on the circle radius. As a consequence, the quantity of product increases linearly in time. We compute explicitly the way the amount of C produced changes with time or with the volume of reactant A injected. We find that geometry can have a profound influence on the efficiency of the reaction such that the radial injection can eventually generate more C under given conditions than the rectilinear case.

To do so, this article first presents the RDA equations describing the spatio-temporal evolution of A + B → C fronts and recalls the initial and boundary conditions specific to the rectilinear and radial geometries. After recalling also the classical scalings of RD A + B → C fronts, we compute the total amount of C produced as a function of time or volume injected in the presence of advection. Rectilinear and radial cases are compared to conclude that the geometrical aspects can be used to optimize the flow control of such reaction fronts.

II. REACTION–DIFFUSION–ADVECTION EQUATIONS

Let us consider a three-dimensional system in which a species A in concentration $\bar{a}_0$ is injected at a constant flow rate $\bar{Q}$ into a domain initially filled with B in concentration $\bar{b}_0$. Upon contact, A and B react to produce C. In the presence of diffusion and advection by a velocity field $\bar{\boldsymbol{v}}$, the spatio-temporal evolution of the dimensional concentrations $\bar{a}, \bar{b},$ and $\bar{c}$ of the reactants A, B, and of the product C, respectively, is the solution of the following RDA equations:

$$\partial_{\bar{t}}\bar{a} + \bar{\boldsymbol{v}}\cdot\nabla\bar{a} = D\nabla^2\bar{a} - k\bar{a}\,\bar{b}, \tag{1a}$$

$$\partial_{\bar{t}}\bar{b} + \bar{\boldsymbol{v}}\cdot\nabla\bar{b} = D\nabla^2\bar{b} - k\bar{a}\,\bar{b}, \tag{1b}$$

$$\partial_{\bar{t}}\bar{c} + \bar{\boldsymbol{v}}\cdot\nabla\bar{c} = D\nabla^2\bar{c} + k\bar{a}\,\bar{b}, \tag{1c}$$

where D is the diffusion coefficient assumed equal for all species and k is the kinetic constant. Normalizing concentrations by $\bar{a}_0$, time by $\tau = 1/(k\bar{a}_0)$, and space by $\ell = (D\tau)^{1/2}$ leads to the dimensionless equations of the problem,

$$\partial_t a + \boldsymbol{v} \cdot \nabla a = \nabla^2 a - a\,b, \tag{2a}$$

$$\partial_t b + \boldsymbol{v} \cdot \nabla b = \nabla^2 b - a\,b, \tag{2b}$$

$$\partial_t c + \boldsymbol{v} \cdot \nabla c = \nabla^2 c + a\,b. \tag{2c}$$

Throughout this article, dimensional and dimensionless variables are denoted with and without a bar, respectively (excepted in the Introduction and Abstract). Depending on the geometry of the reactor and of the injection, different initial and boundary conditions are chosen to solve these equations.

III. RECTILINEAR GEOMETRY

In the rectilinear geometry depicted in Fig. 1(a), the three-dimensional rectangular reactor has an infinite length along the $\bar{x}$ axis, a width $\bar{L}$ along the transverse direction $\bar{y}$, and a height $\bar{h}$ along the third axis $\bar{z}$. The initial condition in dimensionless variables is such that $(a, b, c) = (1, 0, 0)$ for $x \le x_0$ and $(a, b, c) = (0, \gamma, 0)$ for $x > x_0$ where $\gamma = \bar{b}_0/\bar{a}_0$. The initial contact surface between A and B is thus a rectangle of area $\bar{S}_{\text{lin}} = \bar{h}\bar{L}$ located at $x = x_0$. Reactant A is injected along the $\bar{x}$ direction at a constant speed $\bar{v}$ such that the flow rate $\bar{Q} = \bar{S}_{\text{lin}}\bar{v}$ [see Fig. 1(a)]. We assume a hydrodynamically stable, planar displacement with no transverse modulation of the interface along the $\bar{y}$ and $\bar{z}$ axes. The variables depend, therefore, only on $\bar{x}$ and $\bar{t}$ such that the equations governing the dynamics are

$$\partial_t a + v\,\partial_x a = \partial_x^2 a - a\,b, \tag{3a}$$

$$\partial_t b + v\,\partial_x b = \partial_x^2 b - a\,b, \tag{3b}$$

$$\partial_t c + v\,\partial_x c = \partial_x^2 c + a\,b. \tag{3c}$$

The typical shapes of the concentration profiles $a(x, t)$, $b(x, t)$, and $c(x, t)$ and of the production rate $R = ab$ are shown in Fig. 2. Note that, in such a rectilinear geometry, a constant advection speed perpendicular to the front does not affect the dynamics since the problem can be described in the reference frame moving at speed
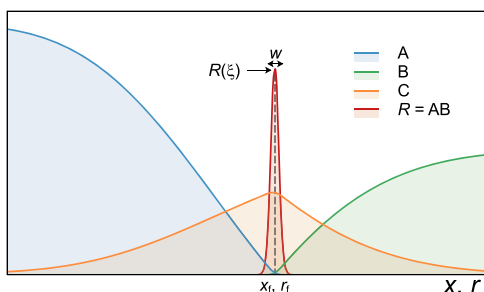
v in which the equations reduce to the RD case considered by Gálfi and Rácz.[7] The role of advection is, thus, trivially to translate, at a constant speed v, the well-known rectilinear RD solutions. Nevertheless, we explicitly consider advection here to be able to compare eventually the properties of the rectilinear RDA front with those obtained in the radial geometry. In particular, we will transform time into injected volume by using the relation $\bar{V} = \bar{Q}\bar{t}$, where $\bar{Q}$ will be the same in both rectilinear and radial cases, in order to compare efficiencies of the injection in converting the reactants into product C depending on the geometry. Let us thus first recall the properties of the rectilinear RDA front and derive the dimensional amount of C produced when an A + B → C front is displaced at a fixed velocity in a rectilinear case.

A. Temporal scalings

Gálfi and Rácz[7] showed that, in the long-time limit and for rectilinear RD fronts, the front position, x_f, the local production rate $R_{\text{lin}}(x_f, t) = a(x_f, t)b(x_f, t)$, and the width w_{lin} of the RD front scale as

$$x_f - x_0 = 2\,\text{erf}^{-1}\left(\frac{1-\gamma}{1+\gamma}\right)t^{1/2} \equiv \alpha_{\text{lin}}(\gamma)\,t^{1/2}, \tag{4a}$$

$$R_{\text{lin}}(x_f, t) = \frac{29}{\pi^4}K_{\text{lin}}^{4/3}\,t^{-2/3} \equiv \beta_{\text{lin}}(\gamma)\,t^{-2/3}, \tag{4b}$$

$$w_{\text{lin}} = \pi K_{\text{lin}}^{-1/3}\,t^{1/6} \equiv \delta_{\text{lin}}(\gamma)\,t^{1/6}, \tag{4c}$$

where

$$K_{\text{lin}}(\gamma) = \frac{(1+\gamma)}{2\sqrt{\pi}}e^{-\alpha_{\text{lin}}^2/4}. \tag{5}$$

The evolution of the coefficients α_{lin}, β_{lin}, and δ_{lin} as a function of γ is shown in Fig. 3(a). We note that, when $\gamma = 1$, i.e., when both reactant solutions have the same initial concentration, we have $\alpha_{\text{lin}} = 0$ and $K_{\text{lin}} = 1/\sqrt{\pi}$. In that case, the front remains stationary at the initial location of contact between the two solutions ($x_f = x_0$) and the production rate and width of the front simply scale as $R_{\text{lin}}(x_f, t) = 29(\pi^7 t)^{-2/3}$ and $w_{\text{lin}} = (\pi^7 t)^{1/6}$. If $\gamma > 1$, i.e., the solution of B is more concentrated than the solution of A, α_{lin} and thus $x_f - x_0$ are negative and the front invades A, whereas $x_f - x_0$ is positive and the front invades B when $\gamma < 1$, i.e., when A is more concentrated. Figure 3(a) also shows that, at a given time t, the amplitude $R_{\text{lin}}(x_f)$ of the production rate distribution increases with increasing values of γ while becoming narrower since its width, w_{lin}, decreases. Nevertheless, the area of the production rate distribution, which is proportional to $R_{\text{lin}}(x_f)w_{\text{lin}} \sim K_{\text{lin}}$, increases with increasing values of γ (see Fig. 4).

B. Total amount of product

The dimensionless total amount $n_{\text{lin,C}}$ of the product generated in the wake of the rectilinear front is given by the integral of the concentration distribution over the whole volume,

$$n_{\text{lin,C}}(t) = \int c(x, t)\,dV = S_{\text{lin}}\int_{-\infty}^{\infty} c(x, t)\,dx, \tag{6}$$

where S_{lin} is the dimensionless area of the rectangular contact zone between the two semi-infinite pools of reactants A and B [Fig. 1(a)].

FIG. 2. Typical concentration profiles of a, b, and c and of the production rate $R = ab$. The amplitude $R(\xi)$ of the production rate is equal to its value at the front position $\xi = x_f$ or $\xi = r_f$ according to the geometry considered. The width, w, of the production rate is also shown.
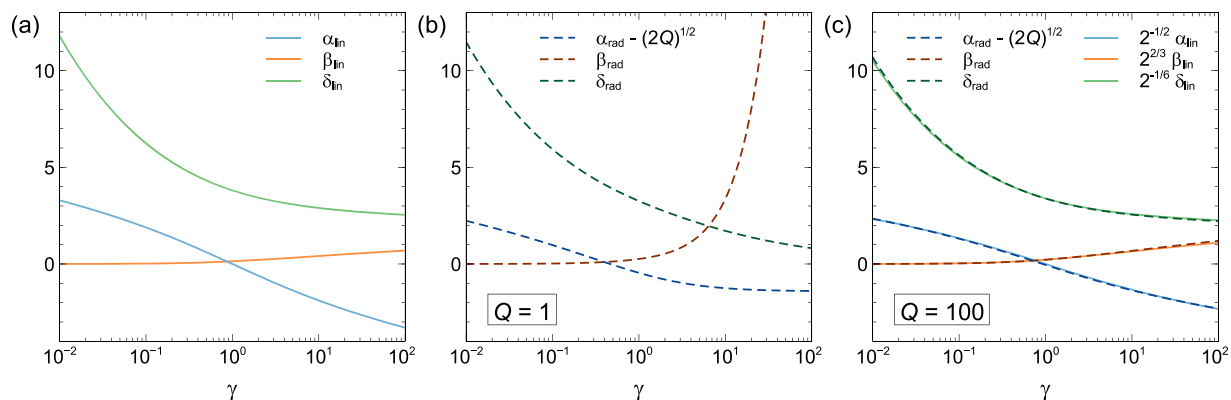
FIG. 3. (a) Evolution of the coefficients α_{lin}, β_{lin}, and δ_{lin} defined by Eq. (4) as a function of γ. Evolution of the coefficients α_{rad}, β_{rad}, and δ_{rad} defined by Eq. (17) as a function of γ for $Q = 1$ (b) and $Q = 100$ (c). The comparison between the radial and the rescaled rectilinear coefficients [see Eq. (20)] is also shown in panel (c).

The last integral can be obtained by integrating Eq. (3c) over x. Noting that the terms related to the transport processes are equal to zero as advection and diffusion do not produce any C, we find

$$\frac{1}{S_{\text{lin}}} \partial_t n_{\text{lin,C}} = \int_{-\infty}^{\infty} R_{\text{lin}} \, dx,$$

expressing the fact that the temporal change of $n_{\text{lin,C}}$ comes from the reaction via the production term R_{lin}. The total amount of product is then obtained by performing the last integration over time, which gives

$$n_{\text{lin,C}}(t) = S_{\text{lin}} \int_0^t dt' \int_{-\infty}^{\infty} R_{\text{lin}}(x, t') \, dx. \tag{7}$$

To compute the integral of the production rate, we note that $R_{\text{lin}}(x, t)$ is a sharply peaked function with a width w_{lin} whose maximum $R_{\text{lin}}(x_f, t)$ is located at $x = x_f$ (see Fig. 2). Therefore, we can write

FIG. 4. Evolution of K_{lin}, defined by Eq. (5), as a function of γ. Inset: Log–Log plot of K_{lin} together with its asymptotic expressions for small and large γ.

$R_{\text{lin}}(x, t) = R_{\text{lin}}(x_f, t) f_{\text{lin}}((x - x_f)/w_{\text{lin}})$, where f_{lin} is a function sharply peaked around its maximum ($f_{\text{lin}}(0) = 1$ and $f'_{\text{lin}}(0) = 0$, where prime is a derivative with respect to the argument). Using the change of variables $\tilde{x} = (x - x_f)/w_{\text{lin}}$, we have

$$\int_{-\infty}^{\infty} R_{\text{lin}}(x, t) \, dx = \eta_{\text{lin}} w_{\text{lin}}(t) R_{\text{lin}}(x_f, t), \tag{8a}$$

where

$$\eta_{\text{lin}} = \int_{-\infty}^{\infty} f_{\text{lin}}(\tilde{x}) \, d\tilde{x} \tag{8b}$$

is a constant related to the precise shape of the production rate R_{lin}. Therefore, using Eq. (8), Eq. (7) becomes

$$n_{\text{lin,C}}(t) = \eta_{\text{lin}} S_{\text{lin}} \int_0^t w_{\text{lin}}(t') R_{\text{lin}}(x_f, t') \, dt'.$$

Using the scalings (4b) and (4c), this last relation gives

$$n_{\text{lin,C}}(t) = \frac{29}{\pi^3} \eta_{\text{lin}} K_{\text{lin}} S_{\text{lin}} \int_0^t (t')^{-1/2} \, dt'$$

$$= \frac{58}{\pi^3} \eta_{\text{lin}} K_{\text{lin}} S_{\text{lin}} t^{1/2} \tag{9}$$

or equivalently

$$n_{\text{lin,C}}(t) = \sigma_{\text{lin}} S_{\text{lin}} t^{1/2}, \tag{10a}$$

$$\sigma_{\text{lin}}(\gamma) = \frac{58}{\pi^3} \eta_{\text{lin}} K_{\text{lin}}(\gamma). \tag{10b}$$

We thus see from Eq. (10a) that the amount of product generated in the course of time in a rectilinear geometry is directly proportional to the area of contact S_{lin} between the two reactant zones and increases as $t^{1/2}$ because of the diffusive growth along the x axis of the contact zone between reactants. It also depends on the reactant concentrations via the ratio γ of their initial values. If $\gamma \ll 1$, $K_{\text{lin}} = \gamma[\ln(1/\gamma\sqrt{2\pi})]^{1/2}$, while in the other limit, $\gamma \gg 1$, we have $K_{\text{lin}} = [\ln(\gamma/\sqrt{2\pi})]^{1/2}$. The evolution of K_{lin} as a function of γ is shown in Fig. 4 together with its two asymptotic expressions. We see that this quantity, and thus the amount of C, increases monotonically with increasing values of γ. This is logical as B is more

concentrated than A and thus readily available to consume any new A injected into the system. On the contrary, if γ is much smaller than 1, then the concentration of A injected is much larger than that of B such that much less C is produced. Note that, using Eqs. (4a) and (5), one can easily obtain the identity

$$K_{\text{lin}}(\gamma) = \gamma K_{\text{lin}}(1/\gamma), \tag{11}$$

which results from the invariance of Eqs. (3) when a and b are exchanged.

Les us now turn to the analysis of the amount of C produced in dimensional variables in order to appreciate how this quantity varies with the volume of the reactant injected.

C. Dimensional total amount of product

In order to discuss the dimensional amount $\bar{n}_{\text{lin,C}}$ of C produced per dimensional injected volume $\bar{V}$ of reactant A, it is convenient to express the dimensionless scaling (10a) in dimensional variables,

$$\frac{\bar{n}_{\text{lin,C}}(\bar{t})}{\bar{a}_0 \ell^3} = \sigma_{\text{lin}} \frac{\bar{S}_{\text{lin}}}{\ell^2} \left(\frac{\bar{t}}{\tau}\right)^{1/2}, \tag{12}$$

where $\bar{n}_{\text{lin,C}}$ is expressed in number of moles. This leads to

$$\bar{n}_{\text{lin,C}}(\bar{t}) = \sigma_{\text{lin}}(\gamma)\,\bar{a}_0 \bar{S}_{\text{lin}}(D\bar{t})^{1/2}. \tag{13}$$

Equation (13) shows that, logically, the larger the value $\bar{a}_0$ of the initial concentration of the reactant A and the larger the surface $\bar{S}_{\text{lin}}$ of the contact area between them, the more C is generated. If the diffusion coefficient D is larger, the flux of reactants toward the reaction front is also larger, which increases $\bar{n}_{\text{lin,C}}$. Note that exchanging the role of a and b should have no impact on the amount of C produced. In this case, we have $\bar{n}_{\text{lin,C}}(\bar{t}) = \sigma_{\text{lin}}(1/\gamma)\,\bar{b}_0\bar{S}_{\text{lin}}(D\bar{t})^{1/2}$. Using the identity (11) together with the definition (10b) of σ_{lin}, we recover Eq. (13) as it should be.

We can finally express the result in terms of the injected volume, $\bar{V} = \bar{Q}\bar{t}$, which will be useful in Sec. V where we compare the total amount of product generated in both geometries,

$$\bar{n}_{\text{lin,C}}(\bar{V}) = \sigma_{\text{lin}}\,\bar{a}_0\bar{S}_{\text{lin}}\left[\frac{D\bar{V}}{\bar{Q}}\right]^{1/2}. \tag{14}$$

In the rectilinear case, the total amount of product formed varies thus as a square root of the volume of reactant injected and scales also as $\bar{Q}^{-1/2}$.

IV. RADIAL GEOMETRY

In the radial geometry shown in Fig. 1(b), the three-dimensional reactor has an infinite length along the $\bar{x}$ and $\bar{y}$ axis, and a height $\bar{h}$ along the third axis $\bar{z}$. In dimensionless variables, the initial condition is such that $(a, b, c) = (0, \gamma, 0)$ everywhere with, here again, $\gamma = \bar{b}_0/\bar{a}_0$. At time $t = 0$, a solution of A in concentration $a_0 = 1$ is injected radially with a constant flow rate at a vertical line, which is the central line of the expanding cylinder of A. In effect, we thus have a two-dimensional model for which the concentration profiles do not depend on the vertical z-axis, as for the rectilinear

geometry. It is then convenient to switch to cylindrical coordinates (r, θ, z) where $r = 0$ is the location of injection. We assume a hydrodynamically stable, radial displacement with no transverse modulation along θ or z such that the velocity field reads $\boldsymbol{v} = (v_r, 0, 0)$ with the radial component $v_r = Q/r$, where Q is the dimensionless flow rate related to the dimensional one through the relation[3]

$$\bar{Q} = 2\pi\bar{h}D\,Q. \tag{15}$$

With those assumptions, the variables of the system depend, therefore, only on r and t. We thus get a one-dimensional problem as for the rectilinear geometry. The dimensionless equations governing the evolution of the concentration fields are obtained from the general equations (2) by using the expression of the velocity field and of the Laplacian operator in cylindrical coordinates,

$$\partial_t a + v_r\partial_r a = (\partial_r^2 + r^{-1}\partial_r)a - a\,b, \tag{16a}$$

$$\partial_t b + v_r\partial_r b = (\partial_r^2 + r^{-1}\partial_r)b - a\,b, \tag{16b}$$

$$\partial_t c + v_r\partial_r c = (\partial_r^2 + r^{-1}\partial_r)c + a\,b. \tag{16c}$$

At later time, the boundary conditions are $a = 1$, $\partial_r b = 0$ at $r \to 0$ and $a = 0$, $b = \gamma$ at $r \to \infty$. Typical concentration profiles $a(r, t)$, $b(r, t)$, and $c(r, t)$, which are similar to those in the rectilinear geometry, are shown in Fig. 2.

A. Temporal scalings

For the radial geometry, we have recently shown that, in the long-time limit, the front position, r_f, along the radial coordinate, the local value of the production rate now defined as $R_{\text{rad}}(r_f, t) = a(r_f, t)b(r_f, t)$, and the width w_{rad} of the RDA front feature the same temporal scalings as in the rectilinear case.[3] We have, indeed, that

$$r_f = 2\mathcal{K}_{\text{rad}}^{1/2}\,t^{1/2} \equiv \alpha_{\text{rad}}(Q, \gamma)\,t^{1/2}, \tag{17a}$$

$$R_{\text{rad}}(r_f, t) = \frac{29}{\pi^4}K_{\text{rad}}^{4/3}\,t^{-2/3} \equiv \beta_{\text{rad}}(Q, \gamma)\,t^{-2/3}, \tag{17b}$$

$$w_{\text{rad}} = \pi K_{\text{rad}}^{-1/3}\,t^{1/6} \equiv \delta_{\text{rad}}(Q, \gamma)\,t^{1/6} \tag{17c}$$

with

$$\mathcal{K}_{\text{rad}}(Q, \gamma) = \mathcal{Q}^{-1}\left(\frac{Q}{2}, \frac{\gamma}{1+\gamma}\right), \tag{18}$$

where $\mathcal{Q}(\mathcal{A}, X) = \Gamma(\mathcal{A}, X)/\Gamma(\mathcal{A})$, $\Gamma(\mathcal{A}, X)$, and $\Gamma(X) = \Gamma(0, X)$ are the regularized incomplete, the incomplete, and the complete gamma functions, respectively.[20] The inverse function $\mathcal{Q}^{-1}(\mathcal{A}, X)$ is the unique solution for Y of the equation $X = \mathcal{Q}(\mathcal{A}, Y)$ ($0 \le X \le 1$, $\mathcal{A} > 0$, and $Y \ge 0$). The coefficient K_{rad} is defined by[3]

$$K_{\text{rad}}(Q, \gamma) = \frac{(1+\gamma)}{\Gamma(Q/2)}\mathcal{K}_{\text{rad}}^{(Q-1)/2}\,e^{-\mathcal{K}_{\text{rad}}}. \tag{19}$$

Note that, even if the temporal scalings are the same as in the rectilinear case, the coefficients α_{rad}, β_{rad}, and δ_{rad} are now a function of the flow rate Q (and of γ), which shows that the flow conditions can be used to control the properties of the front in a radial geometry. The evolution of these coefficients as a function of γ is shown in Figs. 3(b) and 3(c) for two values of the flow rate.

When the flow rate is large, i.e., $Q \gg 1$, simple relationships exist between the coefficients of the rectilinear scalings (4) and those of the radial ones (17). Indeed, as shown in the supplementary material, we then have

$$\alpha_{\mathrm{rad}}(Q, \gamma) = (2Q)^{1/2} + 2^{-1/2}\alpha_{\mathrm{lin}}(\gamma), \quad (20a)$$

$$\beta_{\mathrm{rad}}(\gamma) = 2^{2/3}\beta_{\mathrm{lin}}(\gamma), \quad (20b)$$

$$\delta_{\mathrm{rad}}(\gamma) = 2^{-1/6}\delta_{\mathrm{lin}}(\gamma). \quad (20c)$$

Equation (20a) shows that, at large flow rates, the motion of the RDA front is governed by two distinct contributions. The first term is due to advection and results from a simple volume conservation law: $\bar{V} = \bar{Q}\bar{t} = \pi\bar{r}_f^2\bar{h}$ leading to $r_f = (2Qt)^{1/2}$ by using Eq. (15). The second term is the correction due to the reaction. When both reactants have the same concentration, that is, when $\gamma = 1$, we have $\alpha_{\mathrm{lin}} = 0$ such that $\alpha_{\mathrm{rad}} = (2Q)^{1/2}$ and the front motion is purely advective. If $\gamma < 1$ (A more concentrated than B), $\alpha_{\mathrm{lin}} > 0$ such that $\alpha_{\mathrm{rad}} > (2Q)^{1/2}$ and the front position is then slightly ahead of the position expected from volume conservation, while it is slightly behind it when $\gamma > 1$ and $\alpha_{\mathrm{rad}} < (2Q)^{1/2}$. For sufficiently large flow rates, the radial geometry does not affect much the amplitude R_{rad} and width w_{rad} of the production rate as the coefficients β_{rad} and δ_{rad} are equal to those in the rectilinear case up to a constant scaling factor. Figure 3(c) shows a comparison between the coefficients in the radial case and the rescaled coefficients obtained in a rectilinear geometry. At $Q = 100$, which corresponds to a flow rate $\bar{Q} \simeq 0.04$ ml/min in a reactor of thickness $\bar{h} = 1$ mm (using $D = 10^{-9}$ m^2/s), the simple relationships (20) are already well verified.

Substituting Eqs. (20) into Eqs. (17) and comparing the result with Eqs. (4), we then obtain simple relationships between the rectilinear and the radial dynamics,

$$r_f - (2Qt)^{1/2} = 2^{-1/2}(x_f - x_0), \quad (21a)$$

$$R_{\mathrm{rad}}(r_f, t) = 2^{2/3}R_{\mathrm{lin}}(x_f, t), \quad (21b)$$

$$w_{\mathrm{rad}} = 2^{-1/6}w_{\mathrm{lin}}, \quad (21c)$$

where x_f is the position of the front in the comoving frame or with $Q = 0$ in a rectilinear geometry. Equation (21a) shows that, once the effect of advection has been removed, the motion of the front is slightly slower in the radial geometry compared to the rectilinear geometry. Equations (21b) and (21c) show that the amplitude and width of the production rate should be similar in both geometries, provided they are rescaled properly by constant factors. Figure 5 shows indeed that, upon proper rescaling, both production rates are very similar.

B. Total amount of product

In the radial geometry, the total amount $n_{\mathrm{rad,C}}$ of product C generated in flow conditions has been computed in the long-time limit in the supplementary material of Ref. 3. For the sake of completeness, we recall here the main steps of the calculation. As the concentration profile c is invariant along θ and z, the dimensionless total amount of product is given by
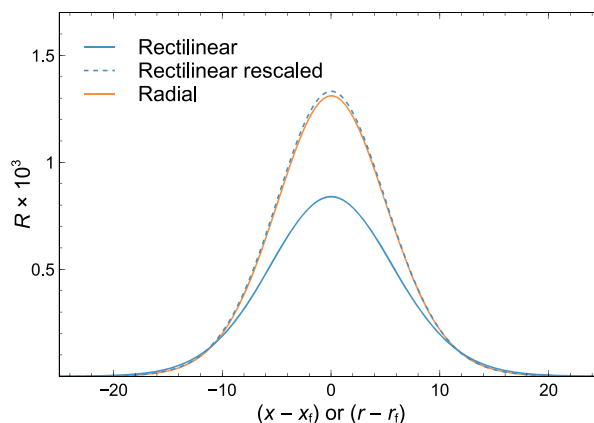
FIG. 5. Production rate profiles in rectilinear and radial geometries at $t = 10^3$ obtained by solving numerically Eqs. (3) and (16) with $Q = 100$ and $\gamma = 1/2$. The dashed profile corresponds to the profile in the rectilinear geometry rescaled using Eqs. (21b) and (21c).

$$n_{\mathrm{rad,C}}(t) = \int c(r, t)d\boldsymbol{r} = 2\pi h\int_0^\infty c(r, t)\, r\, dr. \quad (22)$$

Using Eq. (16c) and recalling that advection and diffusion do not contribute to the production of c, we see that the amount of C produced is related to the production rate as

$$n_{\mathrm{rad,C}}(t) = 2\pi h\int_0^t dt'\int_0^\infty R_{\mathrm{rad}}(r, t')\, r\, dr. \quad (23)$$

To compute the integral over the radial coordinate, we proceed as we did for the rectilinear case by noting that $R_{\mathrm{rad}}(r, t)$ is a sharply peaked function with a width w_{rad} whose maximum $R_{\mathrm{rad}}(r_f, t)$ is located at $r = r_f$ (see Fig. 2). Therefore, we can write $R_{\mathrm{rad}}(r, t) = R_{\mathrm{rad}}(r_f, t)f_{\mathrm{rad}}((r - r_f)/w_{\mathrm{rad}})$, where f_{rad} is sharply peaked around its maximum [$f_{\mathrm{rad}}(0) = 1$ and $f'_{\mathrm{rad}}(0) = 0$, where prime is a derivative with respect to the argument]. Using the change of variables $\xi = (r - r_f)/w_{\mathrm{rad}}$, we have

$$\int_0^\infty R_{\mathrm{rad}}(r, t)\, r\, dr = R_{\mathrm{rad}}(r_f, t)w_{\mathrm{rad}}(t)$$
$$\times \int_{-\frac{r_f}{w_{\mathrm{rad}}}}^\infty f_{\mathrm{rad}}(\xi)[r_f(t) + w_{\mathrm{rad}}(t)\xi]d\xi. \quad (24)$$

Using the scalings (17), we note that, in the long-time limit $t \gg 1$, we have $r_f/w_{\mathrm{rad}} \sim Q^{1/2}t^{1/3}$ such that the lower limit of integration can be replaced by $-\infty$ since the function f_{rad} is sharply peaked around $\xi = 0$ and vanishes quickly when $|\xi| > 0$. In addition, it has been shown that, in the long-time limit, the production rate R is symmetric with respect to its maximum, both in rectilinear[7] and in radial[3] geometries (see also Figs. 2 and 5), such that the integral of $\xi f_{\mathrm{rad}}(\xi)$ on a symmetric interval vanishes. Therefore, Eq. (24) reduces to

$$\int_0^\infty R_{\mathrm{rad}}(r, t)\, r\, dr = \eta_{\mathrm{rad}}R_{\mathrm{rad}}(r_f, t)w_{\mathrm{rad}}(t)r_f(t), \quad (25a)$$

where

$$\eta_{\mathrm{rad}} = \int_{-\infty}^\infty f_{\mathrm{rad}}(\xi)d\xi \quad (25b)$$

is a constant. Consequently, using Eq. (25a), the expression (23) of the total amount of product becomes

$$n_{\mathrm{rad},C}(t) = 2\pi\eta_{\mathrm{rad}}\, h \int_0^t R_{\mathrm{rad}}(r_f, t')\, w_{\mathrm{rad}}(t')\, r_f(t')\, dt',$$

or, equivalently, using Eqs. (17),

$$n_{\mathrm{rad},C}(t) = \frac{116}{\pi^2}\eta_{\mathrm{rad}}\, h\, K_{\mathrm{rad}}(Q,\gamma)\, \mathcal{K}_{\mathrm{rad}}^{1/2}(Q,\gamma)\, t.$$

This last relation can finally be written as

$$n_{\mathrm{rad},C}(t) = \sigma_{\mathrm{rad}}\, 2\pi h\, t, \tag{26a}$$

$$\sigma_{\mathrm{rad}}(Q,\gamma) = \frac{58}{\pi^3}\eta_{\mathrm{rad}}\, K_{\mathrm{rad}}(Q,\gamma)\, \mathcal{K}_{\mathrm{rad}}^{1/2}(Q,\gamma). \tag{26b}$$

Comparison between Eqs. (10) and (26) shows that, despite the analogy of the formulas, we have $n_{\mathrm{rad},C} \sim t$, while $n_{\mathrm{lin},C} \sim t^{1/2}$. This is related to the fact that in the rectilinear case, the advection does not impact the properties of the front such that the amount of C produced is diffusively controlled, imprinting a classical $t^{1/2}$ signature to $n_{\mathrm{lin},C}$. On the contrary, in the radial geometry, the contact area grows as $r_f \sim t^{1/2}$, while diffusion acts also as $t^{1/2}$. Overall, this gives a linear dependence in time of the amount of C generated.

The evolution of σ_{rad} as a function of γ is shown in Fig. 6 for several values of Q. The value of σ_{rad} saturates as γ increases, especially for small Q, indicating a weak possibility to control the yield of the reaction if the initial concentration of B is increased much above that of A. On the contrary, the smaller γ, the smaller σ_{rad}, which shows that the efficiency of the front to produce C decreases when B is much less concentrated than A. Interestingly, the larger the flow rate Q for a given γ, the larger σ_{rad}, which evidences the efficiency of the flow to bring the reactants into contact and thus favor the production of C. In addition, we show in the supplementary material that $\sigma_{\mathrm{rad}} \sim Q^{1/2}$ at large flow rates.
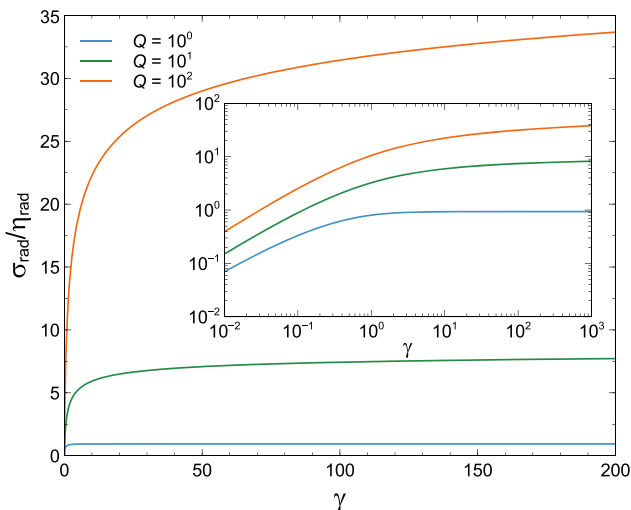
FIG. 6. Evolution of $\sigma_{\mathrm{rad}}/\eta_{\mathrm{rad}}$, defined by Eq. (26b), as a function of γ for several values of Q. Inset: Log–Log plot of $\sigma_{\mathrm{rad}}/\eta_{\mathrm{rad}}$.

C. Dimensional total amount of product

In dimensional variables, Eq. (26a) reads

$$\frac{\bar{n}_{\mathrm{rad},C}(\bar{t})}{\bar{a}_0 \ell^3} = \sigma_{\mathrm{rad}}\, 2\pi \frac{\bar{h}}{\ell}\frac{\bar{t}}{\tau}, \tag{27}$$

leading to

$$\bar{n}_{\mathrm{rad},C} = \sigma_{\mathrm{rad}}\, 2\pi\bar{h}\, \bar{a}_0 D\, \bar{t} = \sigma_{\mathrm{rad}}\, 2\pi\bar{h}\, \bar{a}_0 D\, \frac{\bar{V}}{\bar{Q}}. \tag{28}$$

This equation shows that the amount of C produced logically increases when the initial concentration $\bar{a}_0$, the diffusion coefficient D, or the height of the cell $\bar{h}$ is increased. Similarly, increasing the volume injected $\bar{V}$ produces more C. Interestingly, we also see that, if all parameters are kept constant, less C will be produced if the flow rate $\bar{Q}$ is increased. Indeed, $\sigma_{\mathrm{rad}} \sim Q^{1/2}$ when $Q \gg 1$ and thus $\bar{n}_{\mathrm{rad},C} \sim \bar{Q}^{-1/2}$. This is related to the fact that if the effect of advection becomes more important, then A and B do not have time to meet and react, so less C is generated.

Recalling that, from Eq. (17a), we have $\bar{r}_f/\ell = 2[\mathcal{K}_{\mathrm{rad}}\bar{t}/\tau]^{1/2}$, we can write $\bar{r}_f = 2[\mathcal{K}_{\mathrm{rad}}D\bar{V}/\bar{Q}]^{1/2}$. As the area of the contact zone is given by $\bar{S}_{\mathrm{rad}} = 2\pi\bar{h}\bar{r}_f$, this can also be written as

$$\bar{S}_{\mathrm{rad}} = 4\pi\bar{h}\big[\mathcal{K}_{\mathrm{rad}}D\bar{V}/\bar{Q}\big]^{1/2}. \tag{29}$$

Isolating $\mathcal{K}_{\mathrm{rad}}^{1/2}$ from this expression and replacing this quantity in Eq. (26b) eventually allows us to write (28) as

$$\bar{n}_{\mathrm{rad},C}(\bar{V}) = \tilde{\sigma}_{\mathrm{rad}}\, \bar{a}_0\bar{S}_{\mathrm{rad}}\left[\frac{D\bar{V}}{\bar{Q}}\right]^{1/2}, \tag{30a}$$

where

$$\tilde{\sigma}_{\mathrm{rad}} = \frac{29}{\pi^3}\eta_{\mathrm{rad}}K_{\mathrm{rad}}(Q,\gamma). \tag{30b}$$

Formula (30) show that in the radial case as well, the dimensional amount of C produced grows proportionally to the initial concentration $\bar{a}_0$ of the reactant and to the area $\bar{S}_{\mathrm{rad}}$ of the contact zone between the two reactants. Equation (30a) in the radial geometry is, therefore, formally similar to Eq. (14) in the rectilinear one. However, the important difference between these two relations is that the contact area $\bar{S}_{\mathrm{rad}}$ given by Eq. (29) grows as the radius of the expanding front circle and thus with the volume injected. Therefore, we see finally that the important practical result to recall is Eq. (28), which takes this growth of $\bar{S}_{\mathrm{rad}}$ into account. Nevertheless, Eq. (30) will be useful in Sec. V where we compare the total amount of product generated in both geometries.

V. COMPARISON BETWEEN RECTILINEAR AND RADIAL GEOMETRIES

Comparing Eqs. (10b), (14), and (30), we directly obtain

$$\frac{\bar{n}_{\mathrm{rad},C}}{\bar{n}_{\mathrm{lin},C}} = \frac{1}{2}\frac{K_{\mathrm{rad}}}{K_{\mathrm{lin}}}\frac{\bar{S}_{\mathrm{rad}}}{\bar{S}_{\mathrm{lin}}}\left[\frac{\bar{V}_{\mathrm{rad}}}{\bar{V}_{\mathrm{lin}}}\right]^{1/2}, \tag{31}$$

where $\bar{V}_{\mathrm{rad}}$ ($\bar{V}_{\mathrm{lin}}$) is the volume injected giving rise to a contact area $\bar{S}_{\mathrm{rad}}$ ($\bar{S}_{\mathrm{lin}}$) in the radial (rectilinear) geometry. To obtain Eq. (31), we

have assumed $\eta_{\rm rad} = \eta_{\rm lin}$. Indeed, Fig. 5 shows that this assumption is a good approximation since, upon proper rescaling, the production rates in both geometries are described by essentially the same function such that their integral is very close.

A. Yield per unit area of contact

Equation (31) shows that, in the end, if the same volume of reactant A is injected ($\bar{V}_{\rm rad} = \bar{V}_{\rm lin}$), the production of C per unit area in a radial geometry can be larger or smaller than in the rectilinear case depending on the flow rate Q and the ratio of initial concentrations γ. Indeed, in this case, the link between the radial and rectilinear amounts of C produced per unit area of contact between the reactants is

$$\frac{\bar{n}_{\rm rad,C}}{\bar{S}_{\rm rad}} = \left[\frac{1}{2}\frac{K_{\rm rad}(Q,\gamma)}{K_{\rm lin}(\gamma)}\right]\frac{\bar{n}_{\rm lin,C}}{\bar{S}_{\rm lin}}. \tag{32}$$

If the factor between square brackets is larger than 1, the radial geometry is more effective per unit area to generate the product of the reaction. Figure 7(a) shows that this is the case if, at a given flow rate, γ is larger than a critical value,

$$\gamma^*(Q) \simeq 1.3\, Q^{3/4} e^{3Q/8}, \tag{33}$$

which grows exponentially with Q [see Fig. 7(b)]. Note that, according to Eq. (15), a dimensionless flow rate $Q = 25$ corresponds to a dimensional flow rate $\bar{Q} \simeq 0.01$ ml/min in a reactor with a thickness $\bar{h} = 1$ mm (and $D = 10^{-9}$ m²/s). Therefore, even for moderate
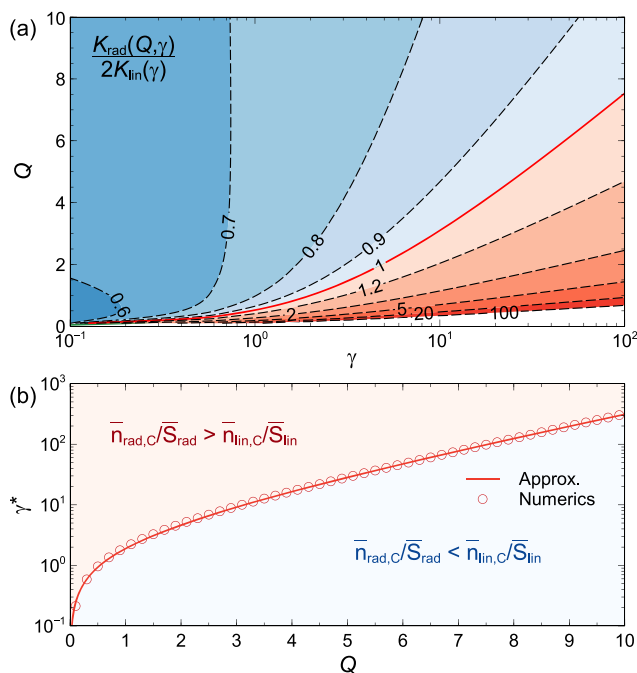
FIG. 7. (a) Contour plot of $K_{\rm rad}/(2K_{\rm lin})$ as a function of Q and γ. (b) Evolution of γ^* for which the yield per unit of area is the same in the rectilinear and radial geometries, i.e., $K_{\rm rad}/(2K_{\rm lin}) = 1$, as a function of Q together with the approximate expression (33).

flow rates as used in many experiments, the rectilinear geometry is intrinsically more efficient than the radial geometry to generate the product of the reaction, provided γ is not too large, i.e., $\gamma < \gamma^*(Q)$. In particular, we show in the supplementary material that, in the limit of large flow rate, i.e., $Q \gg 1$, we have $K_{\rm rad} = \sqrt{2}\,K_{\rm lin}$ such that the value of the factor in Eq. (32) is equal to $2^{-1/2}$ and is thus indeed smaller than 1. The yield of reaction per unit area of contact is thus more favorable at large flow rates in the rectilinear geometry. Nevertheless, in the radial geometry, the growth of the contact area between the two reactants as the injected volume of reactant A increases can eventually compensate the smaller production of C per unit contact area compared to rectilinear geometry and, as shown below, lead to a larger total amount of C generated.

B. Yield per given volume injected

To quantify the difference of product generation on a concrete case, let us compare the amount of product generated for a same volume $\bar{V} = \bar{V}_{\rm lin} = \bar{V}_{\rm rad} = \bar{Q}t$ injected in the two geometries. For the rectilinear geometry, we consider a square reactor of size $\bar{L}$ and thickness $\bar{h}$ such that $\bar{S}_{\rm lin} = \bar{h}\bar{L}$. The experiment is stopped when the front reaches the end of the reactor such that the reactor is completely filled and a volume $\bar{V} = \bar{V}_{\rm max} = \bar{h}\bar{L}^2$ has been injected. For the radial geometry, we consider a square reactor of size $2\bar{L}/\sqrt{\pi}$ and thickness $\bar{h}$ and that the injection is performed at the center of the reactor. Here, the experiment is stopped when the circular front reaches the borders of the square reactor such that the radius $\bar{r}_f = \bar{L}/\sqrt{\pi}$ and the injected volume are the same than in the rectilinear geometry: $\bar{V} = \bar{h}\pi(\bar{L}/\sqrt{\pi})^2 = \bar{h}\bar{L}^2 = \bar{V}_{\rm max}$. In contrast with the rectilinear case for which the contact area remains constant throughout the experiment, the contact area in the radial geometry, $\bar{S}_{\rm rad}$, grows as the injected volume increases. Indeed, using the dimensional form of Eq. (17a), together with $\bar{V} = \bar{Q}t$, we have

$$\bar{S}_{\rm rad} = 2\pi\bar{h}\bar{r}_f = 2\pi\bar{h}\,\alpha_{\rm rad}\sqrt{\frac{D\bar{V}}{\bar{Q}}}.$$

Using $\bar{S}_{\rm lin} = (\bar{V}_{\rm max}\bar{h})^{1/2}$ together with Eq. (15), the ratio between the two contact areas reads

$$\frac{\bar{S}_{\rm rad}}{\bar{S}_{\rm lin}} = \sqrt{2\pi}\,\frac{\alpha_{\rm rad}}{\sqrt{Q}}\sqrt{\frac{\bar{V}}{\bar{V}_{\rm max}}}. \tag{34}$$

Finally, substituting relation (34) into Eq. (31) together with $\bar{V} = \bar{V}_{\rm lin} = \bar{V}_{\rm rad}$, we get

$$\frac{\bar{n}_{\rm rad,C}}{\bar{n}_{\rm lin,C}} = \sqrt{\frac{\pi}{2}}\,\frac{K_{\rm rad}\,\alpha_{\rm rad}}{K_{\rm lin}\,\sqrt{Q}}\sqrt{\frac{\bar{V}}{\bar{V}_{\rm max}}}. \tag{35}$$

Figure 8(a) shows the evolution of the ratio of the dimensional total amount of C generated in radial and rectilinear geometries, given by Eq. (35), as a function of the dimensional volume of reactant A injected for several values of γ and Q. To interpret more easily this evolution, we can use the expression (20a) of $\alpha_{\rm rad}$ together with $K_{\rm rad} = \sqrt{2}\,K_{\rm lin}$, both valid at large flow rates. We then obtain
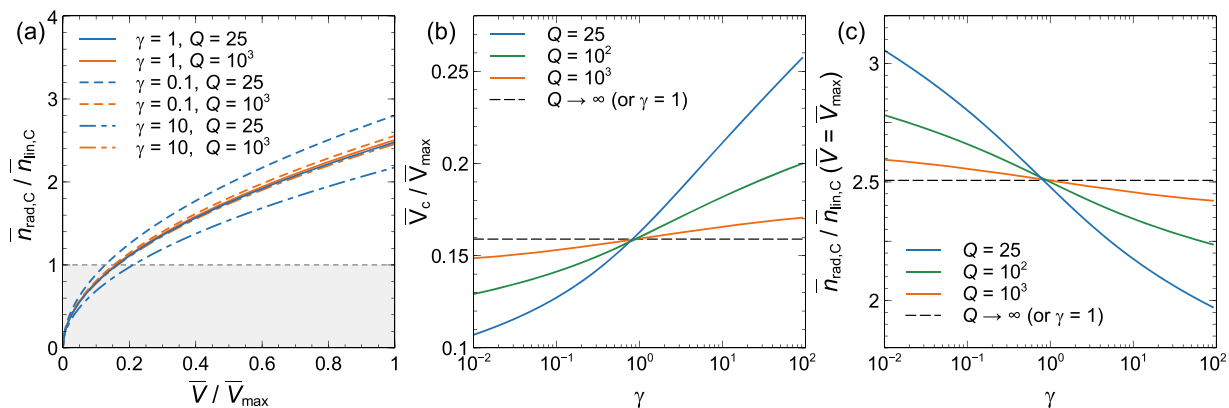
FIG. 8. (a) Evolution of the ratio $\bar{n}_{rad,C}/\bar{n}_{lin,C}$, defined by Eq. (35), as a function of the volume of reactant A injected for several values of γ and Q. $Q = 25$ and $Q = 10^3$ correspond, respectively, to $\bar{Q} \simeq 0.01$ ml/min and $\bar{Q} \simeq 0.4$ ml/min for $\bar{h} = 1$ mm and $D = 10^{-9}$ m^2/s. (b) Evolution of the ratio $\bar{V}_c/\bar{V}_{max}$, defined by Eq. (37), as a function of γ for several flow rates. (c) Evolution of the ratio $\bar{n}_{rad,C}/\bar{n}_{lin,C}$ evaluated at $\bar{V} = \bar{V}_{max}$ [see Eq. (38)] as a function of γ for several flow rates.

$$\frac{\bar{n}_{rad,C}}{\bar{n}_{lin,C}} \underset{Q \gg 1}{=} \left[\sqrt{2\pi} + \sqrt{\frac{\pi}{2Q}} \alpha_{lin}(\gamma) \right] \sqrt{\frac{\bar{V}}{\bar{V}_{max}}}. \qquad (36)$$

When $\gamma = 1$, $\alpha_{lin} = 0$ [see Eq. (4a) and Fig. 3(a)] and the growth of the ratio $\bar{n}_{rad,C}/\bar{n}_{lin,C}$ is independent of the flow rate, provided it is sufficiently large. Indeed, Fig. 8(a) shows that the evolution of this ratio with $\bar{V}$ is essentially insensitive to the value of Q when $\gamma = 1$. When $\gamma < 1$, $\alpha_{lin} > 0$ such that the ratio of C produced is larger compared to the case where $\gamma = 1$. On the contrary, this ratio is smaller compared to the case $\gamma = 1$ when $\gamma > 1$ because $\alpha_{lin} < 0$. We note that the term involving the flow rate in Eq. (36) decreases as the flow rate increases. Therefore, the evolution of the ratio $\bar{n}_{rad,C}/\bar{n}_{lin,C}$ tends to the evolution obtained when $\gamma = 1$ as $Q \to \infty$. This is logical because the reactor is filled more quickly as the flow rate increases, giving less time to the reaction to influence the dynamics. Of course, as Q increases, less product is generated in the reactor.

C. Radial vs rectilinear efficient regimes

Interestingly, Fig. 8(a) also shows that more product C is generated in the radial geometry compared to the rectilinear geometry, i.e., $\bar{n}_{rad,C}/\bar{n}_{lin,C} > 1$, provided the volume injected is larger than some critical value $\bar{V}_c$. Indeed, Eq. (35) can be written as

$$\frac{\bar{n}_{rad,C}}{\bar{n}_{lin,C}} = \sqrt{\frac{\bar{V}}{\bar{V}_c}} \quad \text{with} \quad \frac{\bar{V}_c}{\bar{V}_{max}} = \frac{2 K_{lin}^2 Q}{\pi K_{rad}^2 \alpha_{rad}^2}. \qquad (37)$$

This relation shows that, for two similar experiments for which the same reactants A and B in the same concentration are displaced with the same injection rate, as soon as the injected volume $\bar{V}$ is larger than a critical volume $\bar{V}_c$, the radial geometry produces more C than the rectilinear geometry. If $\bar{V} > \bar{V}_c$, we are thus in a regime where radial injection is most efficient to produce C. Let us call this case the radial efficient regime. On the contrary, if $\bar{V} < \bar{V}_c$, we are in the rectilinear efficient regime for which $\bar{n}_{lin,C} > \bar{n}_{rad,C}$. The existence of this critical volume is expected from the evolution of $\bar{n}_C$ in

both geometries. Indeed, Eq. (14) shows that $\bar{n}_{lin,C} \sim \bar{V}^{1/2}$, whereas Eq. (28) shows that $\bar{n}_{rad,C} \sim \bar{V}$. Therefore, for small enough $\bar{V}$, we should have $\bar{n}_{lin,C} > \bar{n}_{rad,C}$, whereas $\bar{n}_{lin,C} < \bar{n}_{rad,C}$ at large enough $\bar{V}$. Equation (37) rationalizes this argument and gives the volume $\bar{V}_c$ at which the transition occurs as a function of the parameters of the system. The evolution of the ratio $\bar{V}_c/\bar{V}_{max}$ as a function γ is shown in Fig. 8(b) for several flow rates. It shows that the required volume to inject in order to produce more C in a radial geometry grows monotonically as γ increases. However, it has an essentially constant value at $\gamma = 1$, which tends to $\bar{V}_c/\bar{V}_{max} = (2\pi)^{-1} \simeq 0.16$ at large flow rates because $\alpha_{lin}(1) = 0$ [see Eq. (36)]. As the flow rate increases, the evolution of $\bar{V}_c$ becomes flatter and tends to the constant value 0.16 obtained at $\gamma = 1$ and $Q \gg 1$.

At the end of the two experiments, when all reactant A has been injected, i.e., $\bar{V} = \bar{V}_{max}$, we have from Eqs. (35) and (36),

$$\frac{\bar{n}_{rad,C}}{\bar{n}_{lin,C}} = \sqrt{\frac{\pi}{2}} \frac{K_{rad} \, \alpha_{rad}}{K_{lin} \sqrt{Q}} \underset{Q \gg 1}{=} \sqrt{2\pi} + \sqrt{\frac{\pi}{2Q}} \alpha_{lin}. \qquad (38)$$

The evolution of this ratio as a function of γ is shown in Fig. 8(c) for various flow rates. The important feature to note is that this ratio of yields of reaction is always large than one, provided γ is not extremely large (see below). This evidences the efficiency of radial injection over the rectilinear one in producing C. For example, when $\gamma = 1$ and $Q \gg 1$, such that $\alpha_{lin} = 0$, we simply have

$$\bar{n}_{rad,C} = \sqrt{2\pi} \, \bar{n}_{lin,C} \simeq 2.5 \, \bar{n}_{lin,C}. \qquad (39)$$

This shows that the radial geometry can produce 250% more C than the rectilinear geometry in this case. When $\gamma < 1$, such that $\alpha_{lin} > 0$, even more C is produced at the end of the experiment in the radial geometry compared to the case $\gamma = 1$. In contrast, less C is produced, compared to the case $\gamma = 1$, when $\gamma > 1$ because $\alpha_{lin} < 0$. Figure 8(c) also shows that, as the flow rate increases, the evolution of the ratio $\bar{n}_{rad,C}/\bar{n}_{lin,C}$ becomes flatter and tends to the constant ratio obtained when $\gamma = 1$ and $Q \gg 1$.

In all cases reported in Fig. 8(c), more C is produced in the radial geometry compared to the rectilinear geometry. Nevertheless, for a very large γ or low flow rate, the rectilinear geometry can still be more favorable. Indeed, in these cases, the front motion due to the reaction balances advection and prevents the growth of the contact area in the radial geometry such that the rectilinear geometry produces more C. The critical value $\gamma = \gamma_c(Q)$ separating the regimes of radial vs rectilinear optimal efficiency is found by equating the right-hand side of Eq. (38) to 1. The evolution of the numerical solution of this equation as a function of Q is shown in Fig. 9. A simple fit of this evolution can be obtained by using expression (38) valid at large Q together with the definition (4a) of α_{lin} and the expression of the error function valid for large arguments, i.e., $\text{erf}(x) = 1 - e^{-x^2}/(\sqrt{\pi}x)$ for $x \gg 1$.[20] We then obtain $\gamma_c = c_1 Q^{1/2} e^{c_2 Q}$, where c_1 and c_2 are constants. Adjusting those constants leads to the following expression:

$$\gamma_c = 2Q^{1/2} e^{3Q/2}, \tag{40}$$

which fits well with the numerical data, as shown in Fig. 9. We thus see that γ_c grows exponentially with Q such that for $Q = 1$ we obtain $\gamma_c \simeq 9.2$ and for $Q = 10$, we have $\gamma_c \simeq 2.2 \times 10^7$.

Provided $\gamma < \gamma_c(Q)$, we are in the radial efficient regime such that more C is produced in the radial geometry compared to the rectilinear one. This result can be combined with Fig. 7(b) giving the value γ^* comparing the yield per unit area of contact. This allows us to define three regions as shown in Fig. 9. In region (1), probably the most relevant in terms of experimental conditions, more C is produced in the radial geometry compared to the rectilinear case, even if the production per unit area is lower in the radial geometry. In this case, the growth of the contact area in the radial geometry overcomes the lower production per unit area. In region (2), above a first critical value for the ratio of initial concentrations, $\gamma^*(Q)$, more C is produced in the radial geometry and the production per unit area is also larger than the one in the rectilinear geometry. In region (3), above a second critical value, $\gamma_c(Q)$, even if the production per unit area in the radial geometry is larger than the one in the rectilinear
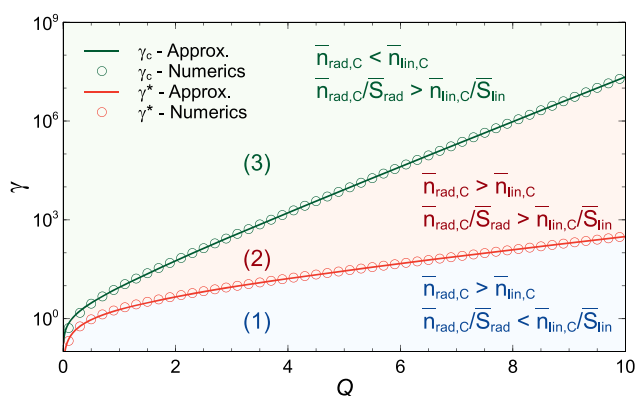
FIG. 9. Evolution of γ_c, defined such that $\bar{n}_{\text{rad,C}} = \bar{n}_{\text{lin,C}}$ when $\bar{V} = \bar{V}_{\text{max}}$, as a function of Q. The approximate expression (40) is also shown. The evolution of γ^* shown in Fig. 7(b) is also displayed, together with the approximate expression (33), and allows us to define the three regions discussed in the text.

geometry, γ is so large and the reaction is so intense that the front cannot grow sufficiently to produce more C than in the rectilinear geometry.

D. Yield per reactor size

Note that in the example of Sec. V B, for the radial geometry, the reactor has an area $4/\pi$ times larger than the one used in the rectilinear geometry. Thus, a slight increase in the reactor size by 27% can lead to a significant increase in produced C (250% for $\gamma = 1$, for example) for a same volume of reactant A injected. If the same reactor of size $\bar{L}$ is used in both geometries, then, at the end of both experiments, $\bar{S}_{\text{lin}} = \bar{h}\bar{L}$ and $\bar{V}_{\text{lin}} = \bar{h}\bar{L}^2$ are unchanged, whereas when $\gamma = 1$ and $Q \gg 1$, $\bar{S}_{\text{rad}} = \pi \bar{h}\bar{L}$ and $\bar{V}_{\text{rad}} = \pi \bar{h}\bar{L}^2/4$ such that Eq. (35) now gives

$$\bar{n}_{\text{rad,C}} = \left[\frac{\pi}{2}\right]^{3/2} \bar{n}_{\text{lin,C}} \simeq 1.97\,\bar{n}_{\text{lin,C}}. \tag{41}$$

The gain is smaller than in the previous case because the injected volume is now smaller in the radial geometry compared to the one in the rectilinear geometry, but the gain is still close to 200%.

Therefore, we see that, even if the production of C per unit area of the interface between A and B can be smaller in the radial geometry than in the rectilinear one, in practice, if γ is not excessively large and/or the flow rate is large enough, the contact area grows sufficiently in time in the radial geometry to overcome this difference at some point and to finally lead to an increased production of C compared to the rectilinear geometry.

To conclude this section, we mention that the study presented in this work is based on long-time analyses that are valid provided the volume injected is sufficiently large, i.e., for sufficiently long time.[3,7] A discussion of the implication in terms of kinetic constant of the reaction is given in the supplementary material.

VI. CONCLUSIONS

We have theoretically compared the properties of A + B → C fronts in, respectively, rectilinear and radial geometries when a solution of A is injected into a solution of B at a constant flow rate. While the scalings in time of the front position, its width, and the local production rate evaluated at the front position are the same in both cases, the coefficients of these scalings can be tuned by the flow rate in the radial case. We explore here the power of this flow control of radial front properties by comparing the yield of the reaction in radial vs rectilinear advection regimes. To do so, we have computed the scalings of the evolution of the amount of product C generated by the reaction as a function of time or volume of the reactant injected. In the rectilinear case, the surface of the contact area between the two solutions remains constant and therefore the dimensional rectilinear amount of product, $\bar{n}_{\text{lin,C}}$, scales as $\bar{t}^{1/2}$, i.e., proportionally to the diffusive growth of the reaction zone. In the radial case, the area of the circular contact zone between A and B increases with the radius of the front circle, which depends primarily on the injection flow rate. As a consequence of this geometrical effect, we find that the radial amount of product $\bar{n}_{\text{rad,C}}$ evolves linearly in time. Similarly, in terms of the dimensional volume injected $\bar{V}$ and dimensional flow rate $\bar{Q}$, we have $\bar{n}_{\text{lin,C}} \sim (\bar{V}/\bar{Q})^{1/2}$ while $\bar{n}_{\text{rad,C}} \sim \bar{V}/\bar{Q}$. Thanks to these differences related to geometry, the radial case can eventually produce

more C for a same volume of reactant A injected or for a reactor of the same size. Indeed, the growth in time of the contact area in the radial geometry can at some point overcome the fact that the production of C per unit area of the contact interface can be smaller in the radial geometry compared to the rectilinear one. We have explicitly computed the critical value $\gamma_c(Q)$ above which the radial injection is more efficient than the rectilinear one in terms of the total amount of C produced per unit area of contact. We have also defined the curve $\gamma^*(Q)$ below which the radial injection yields more product C ultimately, thanks to the radial growth even if the radial yield per unit area of contact is lower than in the rectilinear case.

Future theoretical work could, for instance, address the case of reactants with different diffusion coefficients[21] or other geometries in 2D and 3D for which curvature and advection can influence the yield of the reaction. Experimental work using simple A + B → C chemical reactions should attempt to verify the theoretical predictions proposed here in order to be able to generalize the concept of geometrical control of reaction–diffusion–advection fronts in the wide class of generic A + B → C systems.

SUPPLEMENTARY MATERIAL

See the supplementary material for a detailed derivation of some coefficients of the scalings at large flow rates as well as a discussion of the limit of the long time analysis.

ACKNOWLEDGMENTS

REFERENCES

[1] I. Prigogine and G. Nicolis, *Self-Organization in Nonequilibrium Systems* (John Wiley & Sons, New York, 1977).

[2] J. D. Murray, *Mathematical Biology* (Springer-Verlag, Berlin, 2003).

[3] F. Brau, G. Schuszter, and A. De Wit, "Flow control of A + B → C fronts by radial injection," Phys. Rev. Lett. **118**(13), 134101 (2017).

[4] B. M. Shipilevsky, "Diffusion-controlled formation and collapse of a *d*-dimensional *A*-particle island in the *B*-particle sea," Phys. Rev. E **95**(6), 062137 (2017).

[5] P. M. J. Trevelyan and A. J. Walker, "Asymptotic properties of radial A + B → C reaction fronts," Phys. Rev. E **98**(3), 032118 (2018).

[6] A. Comolli, A. De Wit, and F. Brau, "Dynamics of A + B → C reaction fronts under radial advection in three dimensions," Phys. Rev. E **100**, 052213 (2019).

[7] L. Gálfi and Z. Rácz, "Properties of the reaction front in an A + B → C type reaction-diffusion process," Phys. Rev. A **38**(6), 3151–3154 (1988).

[8] Y.-E. L. Koo and R. Kopelman, "Space- and time-resolved diffusion-limited binary reaction kinetics in capillaries: Experimental observation of segregation, anomalous exponents, and depletion zone," J. Stat. Phys. **65**(5-6), 893–918 (1991).

[9] S. H. Park, S. Parus, R. Kopelman, and H. Taitelbaum, "Gel-free experiments of reaction-diffusion front kinetics," Phys. Rev. E **64**(5), 055102(R) (2001).

[10] I. Lagzi, A. Volford, and A. Büki, "Effect of geometry on the time law of Liesegang patterning," Chem. Phys. Lett. **396**(1-3), 97–101 (2004).

[11] I. Lagzi, P. Pápai, and Z. Rácz, "Complex motion of precipitation bands," Chem. Phys. Lett. **433**(4–6), 286–291 (2007).

[12] M. Dayeh, M. Ammar, and M. Al-Ghoul, "Transition from rings to spots in a precipitation reaction-diffusion system," RSC Adv. **4**(104), 60034–60038 (2014).

[13] B. A. Grzybowski, *Chemistry in Motion: Reaction-Diffusion Systems for Micro- and Nanotechnology* (John Wiley & Sons, New York, 2009).

[14] B. M. Shipilevsky, "Diffusion-controlled annihilation A + B → 0 with initially separated reactants: The death of an *A* particle island in the *B* particle sea," Phys. Rev. E **67**(6), 060101(R) (2003).

[15] B. M. Shipilevsky, "Diffusion-controlled annihilation A + B → 0: The growth of an *A*-particle island from a localized *A* source in the *B*-particle sea," Phys. Rev. E **70**(3), 032102 (2004).

[16] Y. Nagatsu, Y. Ishii, Y. Tada, and A. De Wit, "Hydrodynamic fingering instability induced by a precipitation reaction," Phys. Rev. Lett. **113**(2), 024502 (2014).

[17] F. Haudin, J. H. E. Cartwright, F. Brau, and A. De Wit, "Spiral precipitation patterns in confined chemical gardens," Proc. Natl. Acad. Sci. U. S. A. **111**(49), 17363–17367 (2014).

[18] B. Bohner, G. Schuszter, D. Horváth, and A. Tóth, "Morphology control by flow-driven self-organizing precipitation," Chem. Phys. Lett. **631**, 114–117 (2015).

[19] G. Schuszter, F. Brau, and A. De Wit, "Calcium carbonate mineralization in a confined geometry," Environ. Sci. Technol. Lett. **3**(4), 156–159 (2016).

[20] *NIST Handbook of Mathematical Functions*, edited by F. W. J. Olver, D. W. Lozier, R. F. Boisvert, and C. W. Clark (Cambridge University Press, Cambridge, 2010).

[21] Z. Jiang and C. Ebner, "Simulation study of reaction fronts," Phys. Rev. A **42**(12), 7483–7486 (1990).